Characterisation of a high pH cement backfill for the geological disposal of nuclear waste: The Nirex Reference Vault Backfill

Rita G.W. Vasconcelos[a], Nicolas Beaudoin[b,c], Andrea Hamilton[b], Neil C. Hyatt[a], John L. Provis[a], Claire L. Corkhill[a,*]

[a] NucleUS Immobilisation Science Laboratory, Department of Materials Science and Engineering, University of Sheffield, S1 3JD, UK
[b] Department of Civil and Environmental Engineering, University of Strathclyde, Glasgow, G1 1XJ, UK
[c] School of Geographical and Earth Sciences, University of Glasgow, Glasgow G12 8QQ, UK

ABSTRACT

In a conceptual UK geological disposal facility for nuclear waste within a high-strength, crystalline geology, a cement-based backfill material, known as Nirex Reference Vault Backfill (NRVB), will be used to provide a chemical barrier to radionuclide release. The NRVB is required to have specific properties to fulfil the operational requirements of the geological disposal facility (GDF); these are dependent on the chemical and physical properties of the cement constituent materials and also on the water content. With the passage of time, the raw materials eventually used to synthesise the backfill may not be the same as those used to formulate it. As such, there is a requirement to understand how NRVB performance may be affected by a change in raw material supply. In this paper, we present a review of the current knowledge of NRVB and results from a detailed characterisation of this material, comparing the differences in performance of the final product when different raw materials are used. Results showed that minor differences in the particle size, surface area and chemical composition of the raw material had an effect on the workability, compressive strength, the rate of hydration and the porosity, which may influence some of the design functions of NRVB. This study outlines the requirement to fully characterise cement backfill raw materials prior to use in a geological disposal facility and supports ongoing assessment of long-term post-closure safety.

1. Introduction

Intermediate Level Waste (ILW) comprises a significant proportion, approximately 450 000 m³, of the UK's projected inventory of radioactive waste (Nuclear Decommissioning Authority, 2015). This includes waste arising from the reprocessing of spent nuclear fuel (e.g. spent fuel cladding) and from the operation, maintenance and decommissioning of nuclear facilities (e.g. sludges from the treatment of radioactive liquid effluents) (Hicks et al., 2008). This waste is destined for final disposal in a Geological Disposal Facility (GDF) (Nuclear Decommissioning Authority, 2010a), where the conditioned waste packages will be placed in vaults excavated in host rock, deep underground (Nuclear Decommissioning Authority, 2010b). In a conceptual scenario where a high-strength crystalline rock will host the facility, the vaults will be backfilled with a cement-based material to provide a physical and chemical barrier to radionuclide release (Nuclear Decommissioning Authority, 2010b). For this purpose, the Nirex Reference Vault Backfill (NRVB) has been considered (Francis et al., 1997).

NRVB was designed in the 1990s to fulfil a number of specific requirements for use in a UK geological disposal facility (Francis et al., 1997; Hooper, 1998). These include (Crossland and Vines, 2001; Nuclear Decommissioning Authority, 2010c; United Kingdom Nirex Limited, 2005):

- providing a high alkaline buffered environment, through the dissolution of the different cement hydrate phases by groundwater, to suppress dissolved concentrations of many radionuclides;
- possessing high permeability and porosity to ensure homogeneous chemical conditions, to allow the escape of the gases generated in the GDF and to provide a high surface area for radionuclide sorption; and
- exhibiting low strength to facilitate the possibility of re-excavation of the vaults, if required.

Despite an initial assessment of NRVB at the time of the design and

---

patent (Francis et al., 1997), and subsequently, several assessments of various aspects of this material (e.g. mineralogy, strength, or porosity, as described below), there has not been a comprehensive characterisation of NRVB, where all tests are performed on a consistent batch. Additionally, some of the raw materials used in early development of NRVB are no longer available due to changes in the powder suppliers (Radioactive Waste Management, 2016), therefore, materials to be used when a GDF is in operation may differ in composition and other key characteristics. It is important to understand how the chemical and physical properties of the backfill raw materials may affect the short- and long-term performance of the backfill, to support development of GDF engineering and post-closure safety assessment. We here present a literature review of the published data on NRVB, even where datasets are incomplete, or details pertinent to the analysis of the data are absent.

1.1. NRVB hydration

Portland cement (PC), calcium hydroxide [$Ca(OH)_2$] and calcium carbonate ($CaCO_3$) are the main components of NRVB (Hooper, 1998). The original formulation used a water/solid ratio (w/s) of 0.55 and a water to cement (w/c) ratio of 1.367. According to this composition, Holland and Tearle (2003) described the expected mineralogy of NRVB and the respective changes in relation with temperature. Theoretically, at ambient temperature, the phase assemblage of NRVB is expected to contain calcium hydroxide (also known as portlandite), calcite ($CaCO_3$), calcium silicate hydrate (C-S-H), AFt (ettringite) and AFm (monocarboaluminate) phases, and possibly hydrotalcite if magnesium carbonate is present in the limestone flour or in the Portland cement (Holland and Tearle, 2003). At high temperatures (80 °C), the formation of hydrogarnet-type phases was also predicted, according to thermodynamic modelling (database not specified) performed by the same authors (Holland and Tearle, 2003), although more recent advances in cement chemistry and phase assemblage prediction models indicate that this may be less likely due to the high quantity of carbonate present in this cement formulation. Experimental X-ray diffraction (XRD) performed on fresh (uncured) NRVB revealed that the main phase present was calcite, whereas for NRVB cured for 4 months and 3 years, the phase assemblage was dominated by portlandite (Felipe-Sotelo et al., 2012).

Portlandite and C-S-H are expected to provide the high alkaline-buffering capacity of NRVB. It is proposed that when the backfill material is first in contact with groundwater, the pH will be buffered by the dissolution of the more soluble phases, alkali (i.e. Na, K) hydroxides and sulfates. After the removal of the alkali metal salts, buffering will continue through the dissolution of portlandite; a solution saturated with respect to portlandite is formed with a pH of about 12.5 at 25 °C (Francis et al., 1997). After the portlandite has been exhausted, pH buffering will be maintained by the incongruent dissolution of C-S-H phases with relatively high calcium/silicon molar ratios (Ca/Si), around 1.5. From this, dissolution will result in the release of calcium and hydroxide ions, thus lowering the Ca/Si ratio and reducing the pH value at which the water is buffered (Harris et al., 2002; Hoch et al., 2012). The buffering timescale and capacity of NRVB will depend mainly on the composition and rate of groundwater leaching (Bamforth et al., 2012; Francis et al., 1997). According to a recent study regarding the leaching behaviour of C-S-H using demineralised water, even with a low Ca/Si ratio, the dissolution of C-S-H will buffer the pH to ∼10 (Swanton et al., 2016).

1.2. Physical properties of NRVB

The physical properties of NRVB were summarized by Francis et al. (1997) and Bamforth et al. (2012). The compressive strength of the NRVB (w/s = 0.55) was found to be 4.9 MPa, 5.9 MPa and 6.3 MPa after 7, 28 and 90 days of curing respectively (Francis et al., 1997).

When comparing with compressive strength values obtained for Portland cement (w/s = 0.50), (e.g. 31 MPa, 45 MPa and 46 MPa after 7, 28 and 90 days, respectively, from Menéndez et al. (2003)), the values obtained for NRVB are very low. This relatively low strength thus allows retrievability of waste packages from within NRVB-backfilled vaults (Crossland and Vines, 2001; Nuclear Decommissioning Authority, 2010c; United Kingdom Nirex Limited, 2005).

Since the repository operating temperatures will be higher than the 20 °C used for standard cement curing, studies have been performed to assess the effect of curing temperature (30 °C, 60 °C and 90 °C, cured in moist or excess volume of water) on the strength of NRVB (Francis et al., 1997). Results showed that increasing the temperature of curing corresponds to a reduction in the strength, for example after 28 days of curing at 90 °C, the compressive strength was halved when compared to curing at 30 °C (Francis et al., 1997). Similar results have been obtained with Portland-limestone cement, where a temperature increase negatively influenced compressive strength (Lothenbach et al., 2007). It should be noted, however, that such high curing temperatures (90 °C) are not expected within a GDF vault for ILW.

1.3. Microstructural properties of NRVB

Porosity and permeability must be carefully considered when designing a cementitious material for a GDF, since these properties will influence the transport characteristics of groundwater and radionuclide species through the cement. For example, having a high porosity (more than 30%) allows the ingress of groundwater, dissolution of the different hydrate phases, so providing a high alkaline environment. It also allows the diffusion of gases produced in the waste packages and gives rise to a high surface area, capable of sorbing radionuclide species.

NRVB is relatively porous; the total porosity of NRVB includes a high quantity of unreacted material, was reported to be 50% using mercury intrusion porosity and nitrogen desorption methods, at an unspecified curing age (Francis et al., 1997). However by, comparing the density obtained in dry and water conditions by Francis et al., we can calculate the porosity to be 35%. X-ray computed tomography (XCT) gave a segmented porosity of ∼40% for large scale samples in the non-carbonated region of an NRVB-carbonation trial (Heyes et al., 2015).

After closure, the formation of gases is expected to occur in the GDF, e.g. from corrosion of Magnox cladding, fuel fragments, uranium and steel under anaerobic conditions, microbial degradation of organic compounds and radiolysis of water (Harris et al., 1992). As a result, the permeability of NRVB should be sufficient to allow gas movement without significant over-pressurisation and cracking (Francis et al., 1997). The gas permeability coefficient for argon and helium in NRVB at 28 days of curing (in a membrane of NRVB 20 mm thick, average pressure of 100 kPa) was found to be approximately 2×10^{-15} m^2 in dry conditions and 5×10^{-17} m^2 in saturated grout (Francis et al., 1997; Harris et al., 1992). The average pore radius was determined to be 0.45 μm, with a pore size distribution ranging from 5 nm to > 1 μm (Harris et al., 1992). Harris and colleagues concluded, using the premise that a material is considered to crack if the calculated stress exceeds the tensile strength, that NRVB is able to release gas at a sufficient rate without generating cracks (Harris et al., 1992).

Most of the results presented in the above summary were reported on the basis of unspecified testing methods and precursor materials, and little other detailed information is available about the cement hydration and microstructure of NRVB. Due to the importance of a backfill material in stabilising radioactive waste in a GDF, a thorough understanding of these properties of NRVB is crucial to build a robust post-closure safety case. In this paper, a full characterisation of NRVB is performed. The hydration reaction, the mineralogy and the mechanical properties are studied using two different types of raw materials to assess the implications of security of cement material supply on cement characteristics and performance. These results will have important

Table 1
NRVB formulation (Francis et al., 1997; Hooper, 1998).

Material	Content (kg m^{-3})
CEM I 52.5 N	450
Ca(OH)$_2$/Hydrated lime	170
CaCO$_3$/Limestone flour	495
Water	615

Table 2
Composition of raw materials, as determined by X-Ray Fluorescence analysis (precision ± 0.1 wt%).

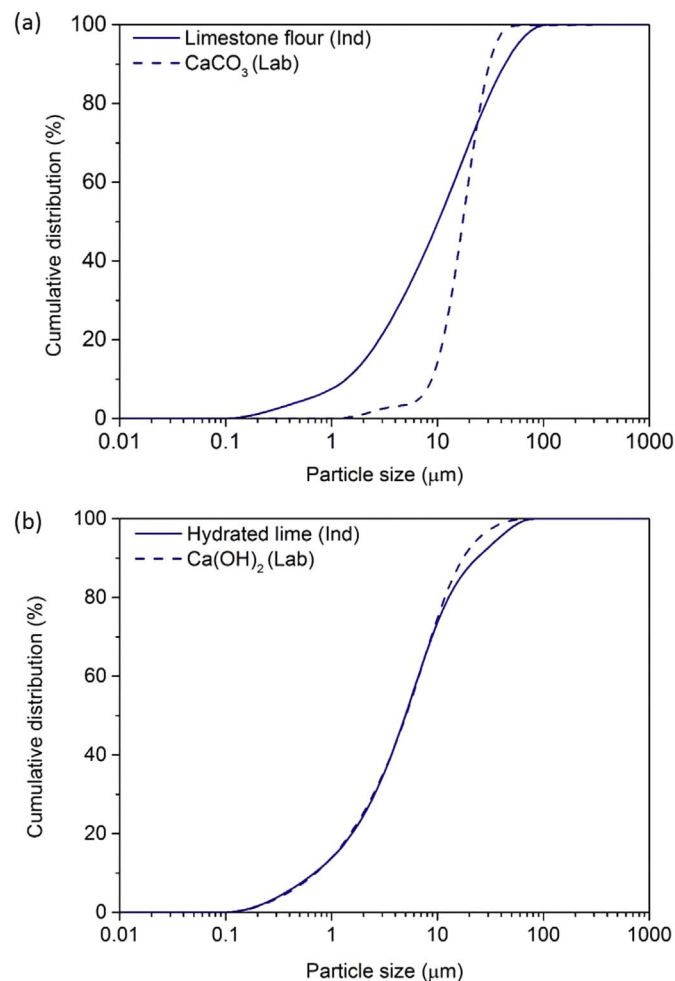| Compound (wt. %)	CEM I 52.5 N	Limestone Flour (Ind)	CaCO$_3$ (Lab)	Hydrated Lime (Ind)	Ca(OH)$_2$ (Lab)
Na$_2$O	0.3	0.2	< 0.1	< 0.1	< 0.1
MgO	1.2	1.6	< 0.1	0.5	0.5
Al$_2$O$_3$	5.2	1.9	< 0.1	< 0.1	0.1
SiO$_2$	19.7	5.4	< 0.1	0.5	0.7
P$_2$O$_5$	0.2	0.1	< 0.1	< 0.1	< 0.1
K$_2$O	0.5	0.3	< 0.1	< 0.1	< 0.1
CaO	64.1	48.1	57.0	73.9	74.5
Fe$_2$O$_3$	2.1	1.7	< 0.1	< 0.1	< 0.1
SO$_3$	–	893 ppm	37 ppm	–	–

Fig. 1. Particle size distribution of (a) CaCO$_3$ and limestone flour and; (b) Ca(OH)$_2$ and hydrated lime.
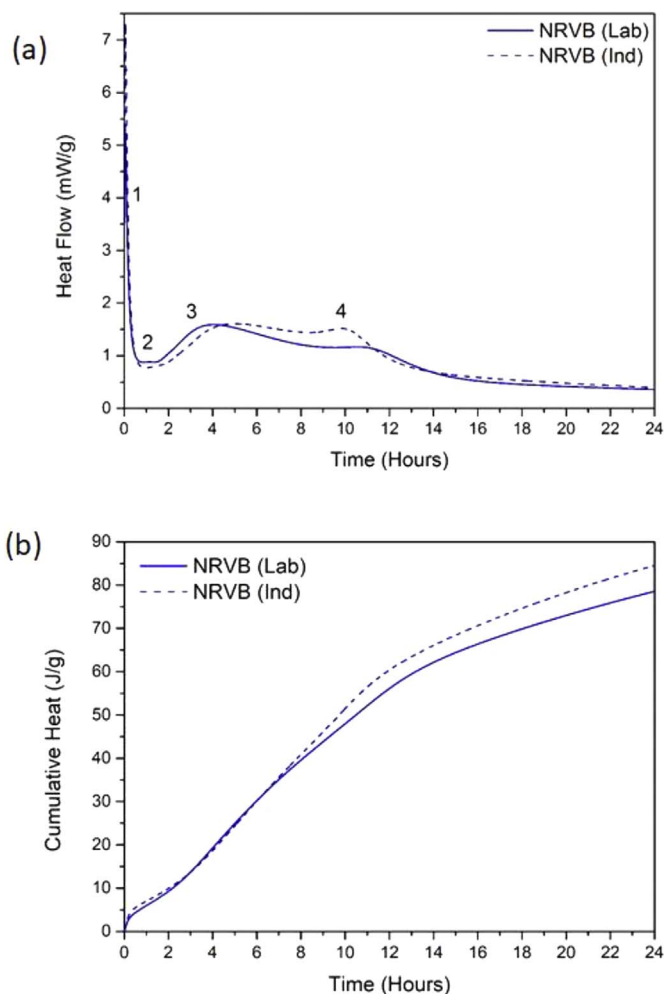

Fig. 2. (a) Isothermal calorimetry of NRVB (Lab) and NRVB (Ind). Thermal features identified are: (1) dissolution and C$_3$A reaction; (2) induction period; (3) reaction of alite and formation of calcium silicate hydrate; (4) sulfate depletion; (b) Cumulative heat of NRVB (Lab) and NRVB (Ind).

implications regarding the applicability of older studies to present day materials in the disposal of nuclear wastes.

2. Materials and methods

2.1. Materials

Batches of NRVB paste were prepared according to the formulation presented in Table 1, with a water/solid ratio (where solid includes all the powder materials used) of 0.55. It is possible to find, in the literature, data pertaining to NRVB prepared with laboratory (pure) materials (e.g. Corkhill et al., 2013) and also with industrial materials (e.g. Butcher et al., 2012). To verify the consistency between the cement formed using these two types of starting materials, two different batches of NRVB were studied. For the NRVB formulated using laboratory chemicals, denoted NRVB (Lab), the starting materials were: CEM I 52.5 N sourced from Hanson Cement Ltd, Ribblesdale works (i.e. Sellafield specification; BS EN 197-1:2011); Ca(OH)$_2$ (≥95.0%) and CaCO$_3$ (≥99.0%) were sourced from Sigma-Aldrich. In the case of NRVB formulated using industrial materials, denoted NRVB (Ind), the following products were used: CEM I 52.5 N (as above); hydrated lime sourced from Tarmac Cement & Lime (Tunstead Quarry, Buxton, UK); and limestone flour sourced from National Nuclear Laboratory (Tendley Quarry, Cumbria, UK; BS EN 13043:2002).

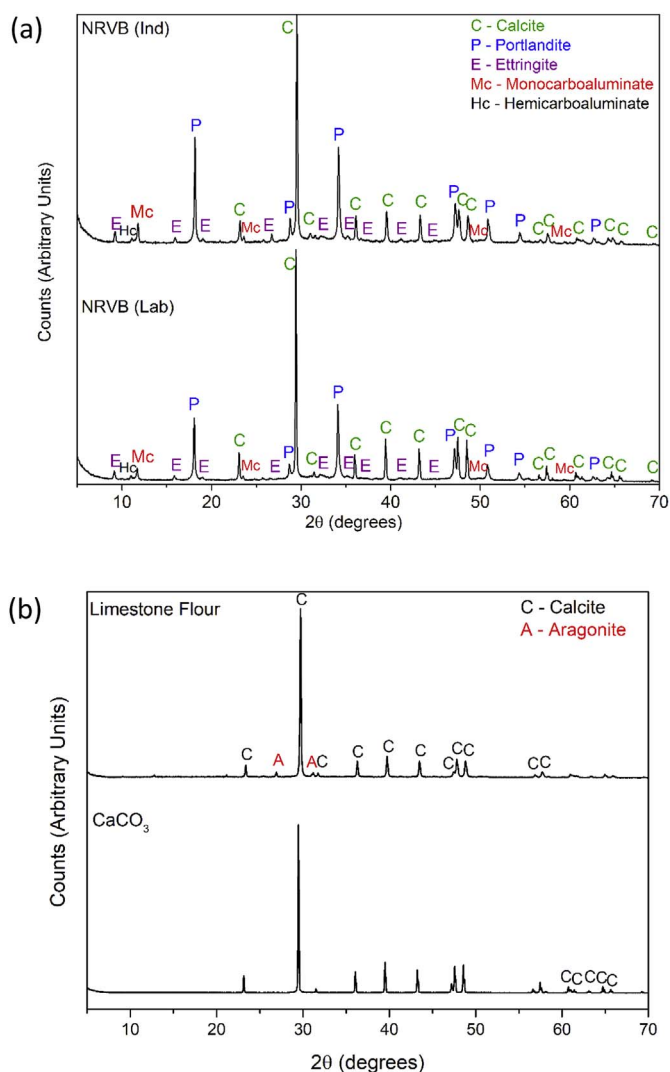The particle size distribution was measured using a Mastersizer

Fig. 3. X-ray diffraction patterns for (a) NRVB (Lab) and NRVB (Ind) after 28 days of curing, and (b) Limestone Flour and CaCO₃. Crystalline phases are labelled.

Fig. 4. TGA-MS for (a) NRVB (Lab); and (b) NRVB (Ind) after 28 days of curing.

3000 PSA, and the results analysed using Malvern Instruments software.

The chemical composition of the starting materials, as calculated using X-ray fluorescence (PANalytical Zetium XRF) of powdered materials, is shown in Table 2. The composition was very similar for both $Ca(OH)_2$ and hydrated lime. However, a slight difference was observed between $CaCO_3$ and limestone flour. For example, $CaCO_3$ contained more CaO than the limestone flour (57 wt% and 48 wt%, respectively). On the other hand, limestone flour presented a higher concentration (between 1.6 and 5.4 wt%) of SiO_2, Fe_2O_3, MgO and Al_2O_3 than reagent grade $CaCO_3$, which contained below 0.05 wt% of these elements (Table 2).

Both cement batches were mixed using a Kenwood benchtop mixer for 5 min. Subsequently, the cement pastes were placed in centrifuge tubes or steel moulds (for compressive strength analysis) and cured at 20 °C and 95% relative humidity, for 28 days.

2.2. Analytical methods

2.2.1. Mechanical properties

The workability of both NRVB formulations was investigated using a mini-slump test (Kantro, 1980). The cement paste was placed in a cone (19 mm top opening x 38 mm bottom opening x 57 mm height) resting on a sheet of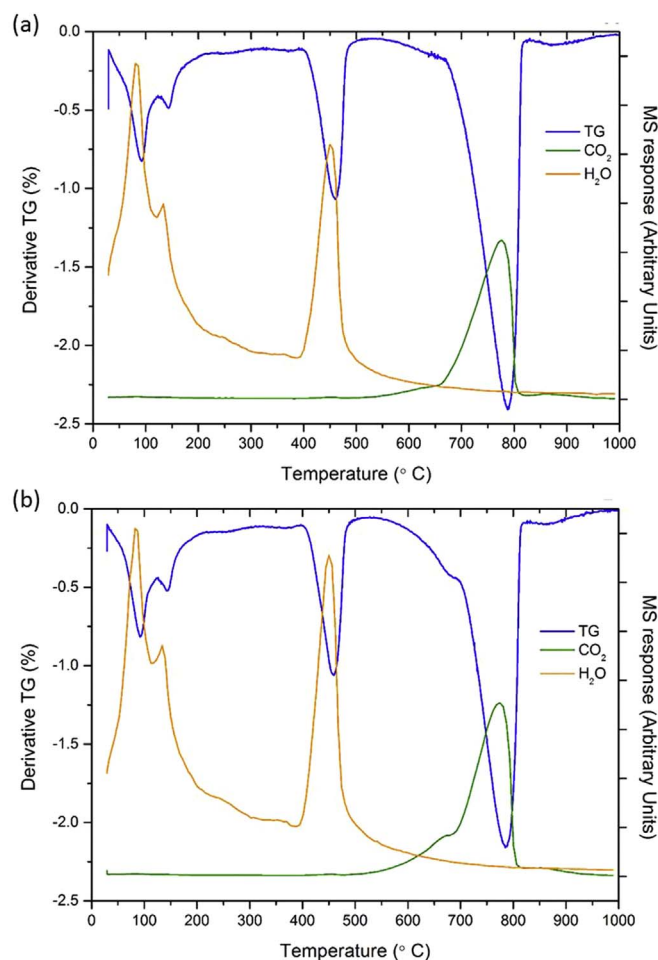 polymethyl-methacrylate. The cone was lifted vertically upwards and the resulting slump area measured using a scale. Each mini-slump test was repeated in triplicate.

The setting time was ascertained using a Vicatronic automatic recording apparatus (Vicat needle method) and 400 g of paste at 19–21 °C and 30–38% relative humidity. The penetration of a needle (1.13 mm diameter) was monitored and the initial setting time was considered as the time when the needle penetration was 35 mm; the final setting time corresponded to less than 0.5 mm of penetration.

After 28 days of curing, compressive strength was measured on cubes with dimensions of 50 × 50 × 50 mm, in triplicate. Cubes were placed within a Controls Automax automatic compressive tester for analysis, with a loading rate of 0.25 MPa/s. The density of both formulations was measured using He pycnometry (Micromeritics AccuPyc II 1340) using approximately 0.40 g of powder (< 63 μm). A fill pressure of 82.7 kPa was purged 50 times over 20 cycles at 25 °C with an equilibration rate of 34.5 Pa/min.

2.2.2. Chemical analysis (hydration)

The heat flow resulting from the NRVB hydration reaction was studied using isothermal calorimetry analysis (TAM Air, TA Instruments) at 20 °C. Approximately 20 g of cement paste was mixed and the measurements were performed for 7 days. As reference sample, tap water was used.

For identification of the hydrate phases present in NRVB at an early age (28 days of curing), XRD and TGA-MS were performed on powder samples (< 63 μm). The former was carried out using a Bruker D2 Phaser diffractometer utilising a Cu Kα source and Ni filter. Measurements were taken from 5° to 70° 2θ with a step size of 0.02° and 2 s counting time per step. For TG-MS analysis, a PerkinElmer Pyris 1
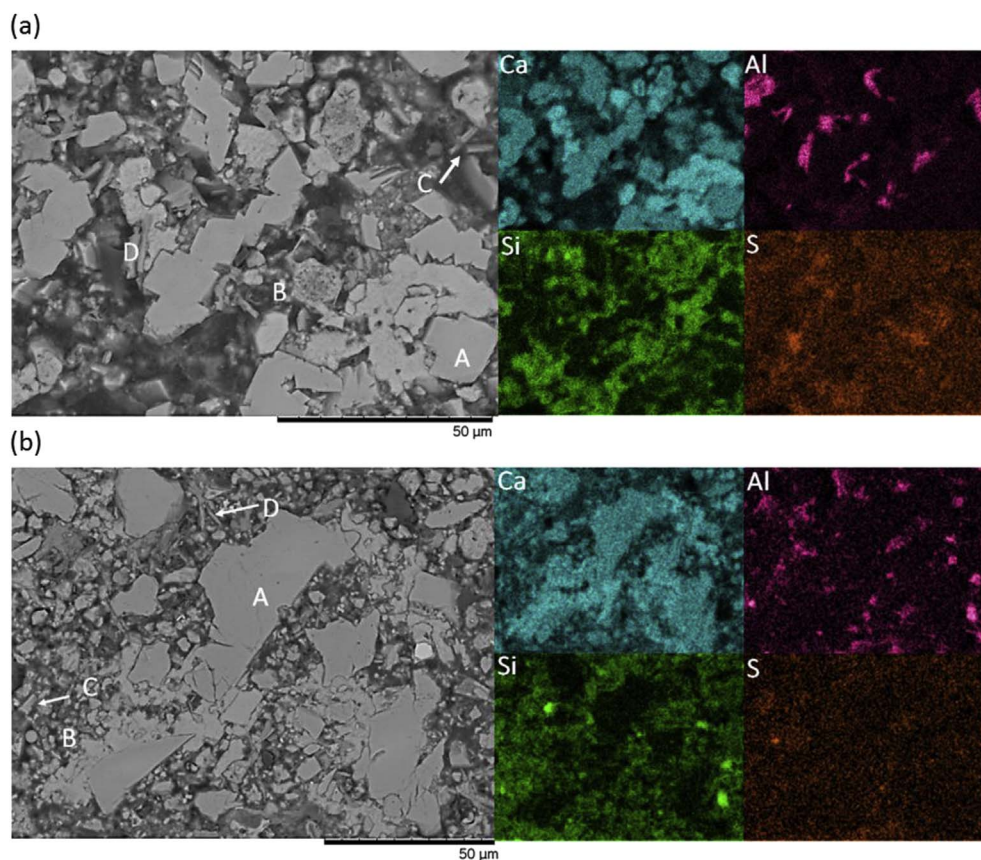
Fig. 5. BSE SEM micrograph of (a) NRVB (Lab) and (b) NRVB (Ind) at 28 days of curing, with the corresponding EDX maps.
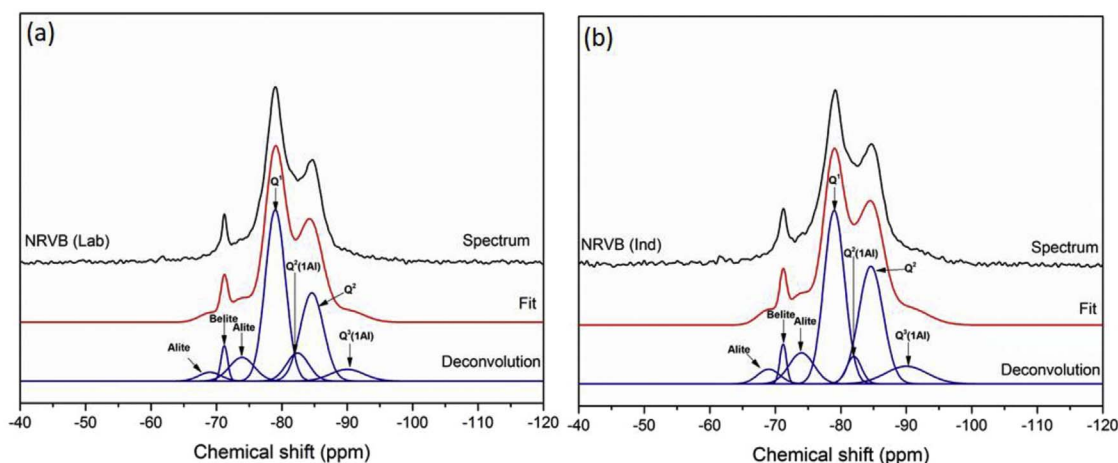

Fig. 6. ^{29}Si MAS NMR spectra, and deconvolution results, for (a) NRVB (Lab) and; (b) NRVB (Ind) after 28 days of curing.

thermogravimetric analyser was used. The temperature ranged from 20 °C to 1000 °C with a heating rate of 10 °C/minute under N_2 (nitrogen) atmosphere. A Hiden Analytical mass spectrometer (HPR-20 GIC EGA) was used to record the mass spectrometric signals for H_2O and CO_2.

Scanning Electron Microscopy (SEM) imaging and Energy Dispersive X-ray (EDX) analysis were performed on NRVB monolith samples mounted in epoxy resin and polished to a 0.25 μm finish using diamond paste. Backscattered electron (BSE) images were recorded using a Hitachi TM3030 scanning electron microscope operating with an accelerating voltage of 15 kV. EDX analysis was performed using Quantax 70 software and elemental maps were collected for 10 min.

Solid-state nuclear magnetic resonance (NMR) spectra for ^{29}Si were collected on a Varian VNMRS 400 (9.4 T) spectrometer at 79.435 MHz using a probe for 6 mm o.d. zirconia rotors and a spinning speed of 6 kHz, a pulse width of 4 μs (90°), a relaxation delay of 2.0 s, and with a minimum of 30000 scans. ^{27}Al NMR spectra were collected on the same instrument at 104.198 MHz using a probe for 4 mm o.d. zirconia rotors and a spinning speed of 12 kHz, a pulse width of 1 μs (25°), a relaxation delay of 0.2 s, and a minimum of 7000 scans.

2.2.3. Microstructure analysis (porosity)

To determine the Brunauer-Emmett-Teller (BET) surface area, nitrogen adsorption-desorption measurements were studied at 77 K on a Micromeritics 3 Flex apparatus. Powder samples of raw material were cooled with liquid nitrogen and analysed by measuring the volume of gas (N_2) adsorbed at specific pressures. The pore volume was taken from the adsorption branch of the isotherm at $P/P_0 = 0.3$. Mercury
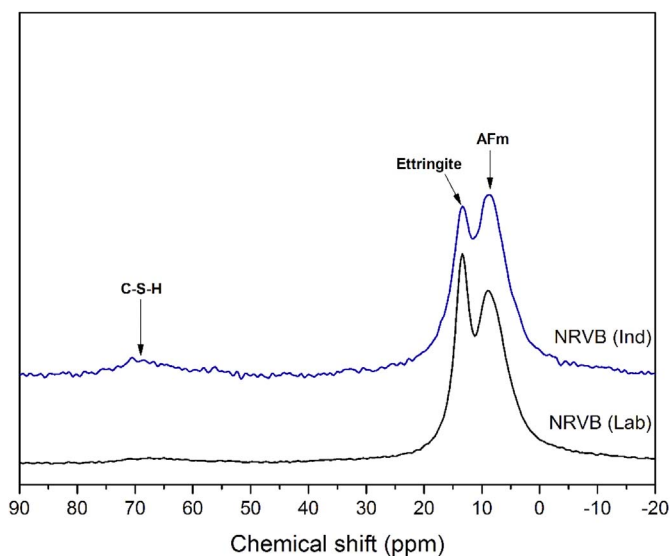
Fig. 7. ^{27}Al MAS NMR spectra of NRVB (Lab) and NRVB (Ind) after 28 days of curing.
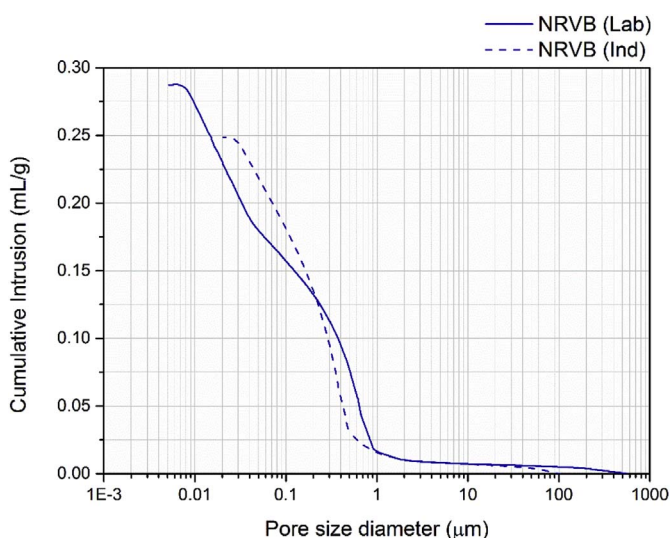

Fig. 8. Pore entry size distribution of NRVB (Lab) and NRVB (Ind) using MIP.

intrusion porosimetry (MIP) was used to study the total porosity and pore distribution of the samples. Small pieces of cement paste were placed into the sample holder of an Autopore V 9600 (Micromeritics Instruments). Washburn's law was used to determine the pore diameter, by applying the following equation: $D = (-4\cos\theta)\gamma/P$, where D is the pore diameter (μm), θ the contact angle between the fluid and the pore mouth (°), γ the surface tension of the fluid (N/m), and P the applied pressure to fill the pore with mercury (MPa). The maximum pressure applied was 208 MPa, the surface tension was 485 mN/m and the contact angle was 130°.

The XCT scans were performed at the University of Strathclyde using a Nikon XTH 320/225 system, equipped with a 225 kV reflection gun, a microfocus multimetal target, and a 2000 × 2000 pixel flat panel photodetector (cell size 0.2 × 0.2 mm). The rotation stage position was set so the X-ray source-to sample distance was minimal and allowed a minimum voxel size of 3 micrometres. Scanning conditions were an accelerating voltage of 100 keV, 28 μA current (corresponding to power 2.8 W) using a silver target. The exposure time for each projection was 2.829 s, lasting 3141 projections (1 frame per projection) and leading to a scan-time of 2.5 h. Gun conditions would not saturate photodetector, consequently no metallic filter was required

during the scans. Projections were overlapped in 3 different heights of the sample with CT Pro 3D software ($^{©}$ 2004–2016 Nikon Metrology) to reconstruct the centre of rotation of the 3D volumes. Once reconstructed, a software built-in algorithmic correction has been applied to correct for artifacts related to beam-hardening (Brooks and Dichiro, 1976). All volumes were reconstructed in 16 bit greyscale, and converted to a.tif stack. A volume of interest (VOI) was selected for each sample, using standards previously reported in the literature, i.e. the VOI should be at least 100 μm^3, or higher than 3 to 5 times the size of the largest distinct feature, to minimise finite size error. In this study, the VOI size chosen was 0.42 mm^3 (250 × 250 x 250 voxels at 3 μm resolution).

3. Results and discussion

3.1. Mechanical properties

The workability, determined by mini-slump testing, of NRVB (Lab) and NRVB (Ind) was found to be 56.5 ± 0.8 mm diameter and 68.4 ± 1.7 mm diameter, respectively. The higher fluidity of NRVB (Ind) is likely related to the difference observed in the particle size distribution between the sources of calcium carbonate (Fig. 1a), where 50% of the particles were smaller than 19.7 μm for CaCO$_3$, and 11.5 μm for limestone flour. For laboratory and industrial grade Ca(OH)$_2$ (Fig. 1b), the particle size distribution was found to be very similar.

For general applications, the initial setting time of a cement should not be less than 45 min, and the final setting time should not be greater than 10 h (Bensted and Barnes, 2008; Taylor, 1997). Using the Vicat method, it was possible to obtain an initial setting time of 5.3 h, and a final setting time of 7.7 h for NRVB (Lab). For NRVB (Ind) the values were very similar, with the initial and final setting times at 5.5 h and 7.3 h. This is in contrast to the initial NRVB formulation study, where an initial setting time of 4.05 h and a final setting of 4.50 h was observed (Francis et al., 1997). Since the w/s ratio in the present study is the same as that used by Francis et al. (1997), this difference is likely to be related to the use of different raw material, and a consequent difference in the reactivity of the materials.

After 28 days of curing, the compressive strength and density of the two materials were compared. The compressive strength was determined to be 8.2 ± 0.2 MPa for NRVB formulated using laboratory materials and 7.15 ± 0.04 MPa for NRVB formulated with industrial materials. This is somewhat greater than that measured by Francis et al. (1997), who found a compressive strength of 5.9 MPa at 28 days for NRVB prepared using components available in the early 1990s. Since no characterisation of these starting materials was published, it is not possible to ascertain which component of this early NRVB formulation gave rise to the reduced strength, although it may be postulated that the 52.5 MPa grade cement used in our trials was of a higher strength grade than the materials used historically, as cement production at this high strength grade was much less common in the early 1990s. The density was determined by helium pycnometry to be 2.251 ± 0.001 g/cm^3 for NRVB (Lab) and 2.328 ± 0.002 g/cm^3 NRVB (Ind); previous measurements of NRVB density using the Archimedes method (100 mm cubes) gave a density of 1.7 g/cm^3 in water-saturated NRVB samples and 1.1 g/cm^3 in oven dried samples (Francis et al., 1997). This lower value could reflect the difference in the methodology used; the Archimedes method determines bulk density, whereas pycnometry allows the determination of solid density as helium gas reaches all of the pores within the cement.

3.2. Chemical analysis (hydration)

Fig. 2a shows the isotherm generated for both NRVB formulations during hydration. It is possible to identify the four main hydration stages, as observed in a plain Portland cement. In comparison to Portland cement, the heat flow was lower (Fig. 2b) by a factor of ~2
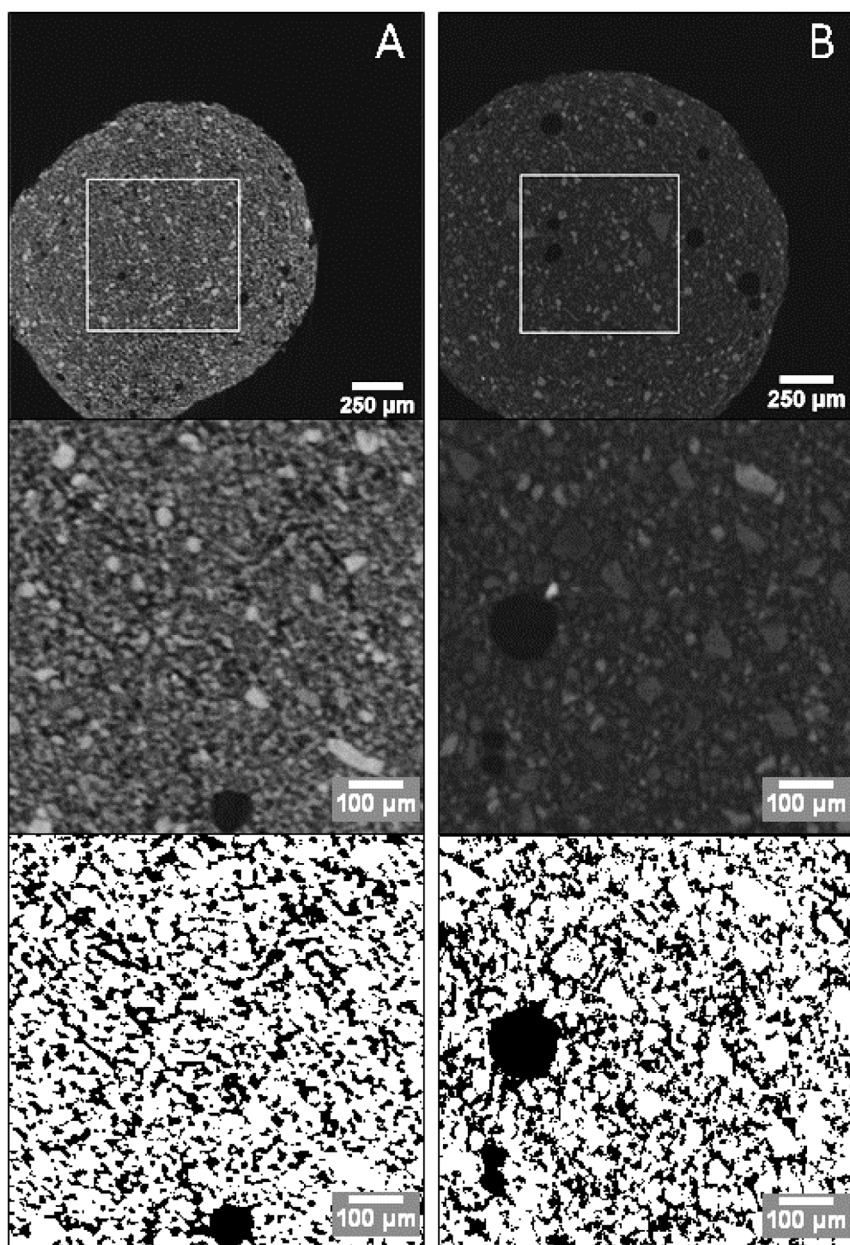
Fig. 9. XCT data of (a) NRVB (Lab) and (b) NRVB (Ind). Top: Slices through the tomographic reconstruction, showing the selected VOI (square); centre: selected slices through the VOI in each sample; and bottom: segmented into solid (white) and pore (black) regions.

(Jansen et al., 2012). This is related to the much lower fraction of material undergoing hydration in the NRVB formulation. Comparing the two formulations of NRVB, it can be observed that the heat flow was very similar, however one subtle difference was observed: the curve corresponding to the sulfate depletion period (labelled 4, Fig. 2a) of NRVB (Ind) indicates that it evidenced a more intense reaction than NRVB (Lab). One possible explanation is the formation of additional calcium monocarboaluminate hydrate in NRVB (Ind) as observed in XRD and NMR data (discussed below). In accordance with the particle size analysis (Fig. 1a), determination of the surface area of the $CaCO_3$ sources indicated that the limestone flour used in NRVB (Ind) had a significantly higher surface area than $CaCO_3$ used in NRVB (Lab), with values of 5.2 ± 0.2 m^2/g and 3.7 ± 0.2 m^2/g, respectively. The higher surface area is responsible for a higher rate of calcite dissolution and also the availability of more nucleation sites, resulting in the formation of more hydration products (Scrivener et al., 2015). Another factor to consider is the higher content of sulfate present in the industrial raw material, which may give rise to the observed differences; the limestone flour of NRVB (Ind) had 893 ppm sulfur, compared with

37 ppm in the hydrated lime of NRVB (Lab) (Table 2).

The main phases identified in the NRVB formulations by X-ray Diffraction (XRD) were calcite ($CaCO_3$; PDF 01-086-0174) and portlandite (Ca(OH)$_2$; PDF 01-072-0156) (Fig. 3a). Ettringite ($Ca_6Al_2(OH)_{12}(SO_4)_3 \cdot 26H_2O$; PDF 00-041-1451), calcium monocarboaluminate hydrate ($Ca_4Al_2(OH)_{12}(CO_3)_3 \cdot 5H_2O$; PDF 01-087-0493) and calcium hemicarboaluminate hydrate ($Ca_4Al_2(OH)_{12}$ [OH (CO$_3$)$_{0.5}$]$\cdot 5.5H_2O$; PDF 00-041-0221) were also identified. These results are in agreement with those identified previously in NRVB cured at ambient temperature (Felipe-Sotelo et al., 2012). While the phase assemblage for each formulation was similar, subtle differences were observed in the peak intensities of several reflections; monocarboaluminate reflections were more intense in NRVB (Ind) than NRVB (Lab), while reflections of calcite were more intense in NRVB (Lab), which is also apparent in the XRD patterns corresponding to limestone flour and $CaCO_3$ (Fig. 3b). These differences may be attributed to the chemical composition, particle size distribution and surface area of the $CaCO_3$ and limestone flour, however, preferential orientation cannot be ruled out, especially for layered or platy phases such as

monocarboaluminate and portlandite.

TG-MS analysis confirmed the presence of the phases identified by XRD (Fig. 4). The two peaks between 100 and 200 °C can be attributed to the presence of ettringite and monocarboaluminate, while the peaks between 400 and 500 °C, and 650–800 °C correspond to portlandite and calcite, respectively (Lothenbach et al., 2007; Sun, 2011). The same peaks were observed for both formulations, however for the NRVB (Ind) (Fig. 4b) an additional peak was observed at ∼ 650 °C, corresponding to the presence of magnesian calcite and supported by the presence of a greater quantity of Mg in NRVB (Ind) than NRVB (Lab) (Table 2).

Through SEM imaging and EDX analysis it was possible to identify the microstructure of the different hydrate phases, as shown in Fig. 5. The large Ca-containing rhombohedral crystals (labelled A, Fig. 5) are portlandite. The Ca and Si-rich phase surrounding portlandite crystals (labelled B, Fig. 5) may be C-S-H. The areas containing higher concentrations of aluminium (labelled C, Fig. 5) suggest the presence of AFm phases. The areas labelled D are indicative of the presence of sulfate-containing AFm phases and/or ettringite, due to the higher concentration of both aluminium and sulfate. Comparing the SEM images of the two formulations, it is possible to identify the same hydrate phases, however the matrix of NRVB formulated with industrial materials has a more fine grained morphology, consistent with the analysis of limestone flour.

In the ^{29}Si MAS NMR spectra (Fig. 6) it was possible to identify some unreacted Portland cement through the presence of alite (chemical shifts −69 and −73.9 ppm) and belite (−71.2 ppm) (Scrivener et al., 2016) in both NRVB formulations. Contributions from Q^1 (−79 ppm), $Q^2(1Al)$ (−83 ppm) and Q^2 (−84 ppm) silicate environments were also observed in both formulations; these chemical shifts are characteristic of C-S-H (Richardson, 2008; Richardson et al., 2010). A small resonance was also observed at −90 ppm corresponding to $Q^3(1Al)$. The presence of Al shows the incorporation of this element in the C-(A)-S-H (Richardson et al., 2010). Comparison of the two formulations reveals a small difference in the spectra (Fig. 6a and b) between NRVB (Lab) and NRVB (Ind); this is related to the intensity of Q^2 (−84 ppm), $Q^2(1Al)$ (−83 ppm) and Q^3 (1Al) (−90 ppm). A possible reason is the difference observed in the reactivity of the raw materials used in the two formulations, specifically the higher surface area of the limestone flour.

Fig. 7 shows the ^{27}Al NMR spectra of NRVB (Lab) and NRVB (Ind). The small peak observed at approximately −69 ppm (more evident for NRVB Ind) is attributed to the substitution of Al for Si in C-S-H (Lothenbach et al., 2008), in agreement with the observation of small peaks corresponding to $Q^2(1Al)$ and $Q^3(1Al)$ in the ^{29}Si MAS NMR spectra (Fig. 6). The peaks visible at approximately +13 and +9 ppm indicate the presence of octahedrally coordinated Al in ettringite and AFm phases. As stated previously in the literature (Lothenbach et al., 2008), it is not possible to distinguish between the different AFm phases due to the similar chemical shift. Comparing the two formulations, it is possible to see a difference in the proportion of ettringite and AFm phases present; the presence of more AFm in NRVB (Ind) is related to the higher availability of dissolved carbonate (higher surface area) and consequent formation of monocarboaluminate, in accordance with the results observed by isothermal calorimetry (Fig. 2a) and XRD (Fig. 3a).

3.3. Microstructure (porosity)

A two-fold approach was applied to determine the porosity of the two NRVB formulations, to ensure all pore sizes were considered in the analysis. Mercury Intrusion Porosimetry, where it is understood that the pore diameters obtained correspond to the pore entry size and not the real size of the pore (Scrivener et al., 2016), was performed to compare the trend and changes in the pore size distribution between the two NRVB formulations (Diamond, 2000). Fig. 8 shows the pore entry size diameter in relation to the cumulative intrusion for NRVB (Lab) and NRVB (Ind). The curve for NRVB (Lab) allocates essentially all of the pores to threshold pore entry radii below 0.8 μm, whereas for NRVB

(Ind) the curve allocates all of the pores to sizes below 0.5 μm. This small difference is also evident in the total porosity obtained, where for NRVB (Lab) the percentage of total porosity obtained was 38 ± 1% and for NRVB (Ind) was 32 ± 1%. It is important to note that, due to the low compressive strength of NRVB (around 8 MPa), this technique (which reaches pressures of 208 MPa in the instrument used in this study) might not be suitable to use to quantify the finer pores due to the potential for collapse of pores during analysis. This is expected to occur at ∼0.14 mL/g of intrusion for NRVB (Lab) and at ∼0.15 mL/g for NRVB (Ind) based on the strength data.

X-ray Computed Tomography was also used to study the porosity of NRVB. This technique has the advantage of being non-invasive and to allow three-dimensional reconstructions, but has limitations in spatial resolution. Fig. 9 shows selected slices of the VOI for the two samples analysed. Quantitative analysis was performed using segmentation of the VOI. A threshold value was chosen based on the line shape of the image histograms, which show peaks of higher and lower absorption voxels, where the lower absorption voxels correspond to surrounding air and internal void space (Landis and Keane, 2010), allowing discrimination between pore space and binder phases (solid). The MIP results were used to guide the thresholding process, so the comparison between the results obtained by the two techniques is to some degree influenced by this.

No cracks were observed in the samples at this early age (28 days of hydration). The porosities obtained from tomographic data were 39% for NRVB (Lab) and 35% for NRVB (Ind). This difference is related, once more, to the difference observed in the hydration reaction of both cements, due to the smaller particle size and higher surface area of limestone flour.

The porosity results are in the same range presented by Heyes et al. (2015) (∼40%), however they are lower than those reported by Francis et al. (1997), where the porosity measured using MIP and nitrogen desorption was around 50%. It is important to note, however, that by estimating the porosity using the density values measured in Francis et al. (∼35%), the results obtained in this paper are very similar. Differences in the characteristics between the raw materials used in the 1990's and those used in the present study are likely to be responsible for the differences observed.

3.4. Influence of precursor materials on NRVB characteristics and properties

In summary, the differences in the surface area and chemical composition of the raw materials, particularly $CaCO_3$ and limestone flour, impacted the properties of the NRVB formulations. In addition to differences between the NRVB formulations investigated here, we also observed differences between the results obtained in this study when compared to the characterisation performed in the early 1990's, likely due to differences in the raw material and other unspecified properties. The impact of raw material selection on properties required for geological disposal are discussed below.

Workability, compressive strength and setting time were affected by the use of different raw materials. In the present study, the higher surface area of limestone flour resulted in a higher workability and lower compressive strength for NRVB formulated with industrial raw materials when compared to NRVB formulated with laboratory raw materials. When comparing our data with those from the early 1990's (Francis et al., 1997), the workability and setting time were a factor of ∼1.5 lower in the present study, which we attribute to differences in fineness of the precursor materials used. The differences observed should not strongly influence the ability for the backfill to be poured within vaults, and the compressive strength values obtained are low enough to allow re-excavation of the vaults if necessary.

With regards to the long-term behaviour of NRVB, differences in the rate of hydration, the quantity of different hydrate phases, and the hydrate phase assemblage may influence the buffering capacity of the

material. In the present study, the rate of hydration was faster in NRVB formulated with industrial raw materials due to the high surface area of limestone flour. The quantity of monocarboaluminate was also greater, which is a consequence of the higher availability and reactivity of dissolved carbonate in limestone flour. Furthermore, small differences in the chemical composition of limestone flour, for example, the presence of S (and, to a lesser extent, Mg) influenced the rate of hydration. This may have implications for the hydrate phase assemblage at timescales longer than 28 days of curing; further work is required to investigate this.

Through ^{29}Si MAS NMR spectroscopy we have shown the incorporation of aluminium in the C-(A)-S-H of NRVB, and that the choice of raw material influences the quantity incorporated (Figs. 6 and 7). Previous studies have shown that aluminium incorporated into amorphous silica reduces the dissolution rate, even in high alkaline environments (Chappex and Scrivener, 2013, 2012; Iler, 1973). Therefore, the buffering behaviour of the repository may not occur on the predicted time scale, or result in a pH comparable to that estimated when considering C-S-H dissolution only (Nuclear Decommissioning Authority, 2010b).

Finally, we observed that the choice of raw material also influences the 28-day porosity of the final NRVB, which is associated with the differences in hydration reaction outlined above; the formation of more hydrate products in NRVB formulated with industrial materials resulted in a slightly lower porosity. In a repository environment, such a difference may strongly influence the rate of groundwater ingress and the egress of gas, which are key design functions of NRVB.

4. Conclusion

The use of different raw materials in the synthesis of NRVB has been investigated, and the differences in workability, setting time, hydration and porosity analysed. These results are compared with those previously reported in the literature for this material, and the potential effects of differences in raw materials on the final use of NRVB have been explored. Surface area, fineness and chemical composition of the raw materials, particularly limestone flour, have been shown to influence, to a small extent, final backfill properties including setting time, compressive strength and buffering capacity. The effects on porosity seem to be significant, but this may also be due to differences in analysis techniques applied to investigate this property. This study highlights the importance of a detailed characterisation of raw materials used in the formulation of NRVB for use in a geological disposal facility, especially in light of concerns surrounding security of cement supply for future applications.

Acknowledgements

References

Bamforth, P.B., Baston, G.M.N., Berry, J.A., Glasser, F.P., Heath, T.G., Jackson, C.P., Savage, D., Swanton, S.W., 2012. Cement materials for use as backfill, sealing and structural materials in geological disposal concepts. In: A Review of Current Status. SERCO/005125/001 Issue 3.

Bensted, J., Barnes, P., 2008. Structure and Performance of Cements, second ed. Taylor & Francis e-Library.

Brooks, R., Dichiro, G., 1976. Beam hardening in X-ray reconstructive tomography. Phys. Med. Biol. 390–398.

Butcher, E.J., Borwick, J., Collier, N., Williams, S.J., 2012. Long term leachate evolution during flow-through leaching of a vault backfill (NRVB). Mineral. Mag. 76, 3023–3031. http://dx.doi.org/10.1180/minmag.2012.076.8.18.

Chappex, T., Scrivener, K.L., 2013. The effect of aluminum in solution on the dissolution of amorphous silica and its relation to cementitious systems. J. Am. Ceram. Soc. 96, 592–597. http://dx.doi.org/10.1111/jace.12098.

Chappex, T., Scrivener, K.L., 2012. The influence of aluminium on the dissolution of amorphous silica and its relation to alkali silica reaction. Cem. Concr. Res. 42, 1645–1649. http://dx.doi.org/10.1016/j.cemconres.2012.09.009.

Corkhill, C.L., Bridge, J.W., Chen, X.C., Hillel, P., Thornton, S.F., Romero-Gonzalez, M.E., Banwart, S. a., Hyatt, N.C., 2013. Real-time gamma imaging of technetium transport through natural and engineered porous materials for radioactive waste disposal. Environ. Sci. Technol. 47, 13857–13864. http://dx.doi.org/10.1021/es402718j.

Crossland, I.G., Vines, S.P., 2001. Why a cementitious repository. Nirex Report N/034.

Diamond, S., 2000. Mercury porosimetry: an inappropriate method for the measurement of pore size distributions in cement-based material. Cem. Concr. Res. 30, 1517–1525. http://dx.doi.org/10.1016/S0008-8846(00)00370-7.

Felipe-Sotelo, M., Hinchliff, J., Evans, N., Warwick, P., Read, D., 2012. Sorption of radionuclides to a cementitious backfill material under near-field conditions. Mineral. Mag. 76, 3401–3410. http://dx.doi.org/10.1180/minmag.2012.076.8.53.

Francis, A.J., Cather, R., Crossland, I.G., 1997. Nirex Safety Assessment Research Programme: Development of the Nirex Reference Vault Backfill; Report on Current Status in 1994. Report no: S/97/014. .

Harris, A.W., Atkinson, A., Claisse, P.A., 1992. Transport of gases in concrete barriers. Waste Manag. 12, 155–178.

Harris, A.W., Manning, M.C., Tearle, W.M., Tweed, C.J., 2002. Testing of models of the dissolution of cements - leaching of synthetic CSH gels. Cem. Concr. Res. 32, 731–746. http://dx.doi.org/10.1016/S0008-8846(01)00748-7.

Heyes, D.W., Butcher, E.J., Borwick, J., Milodowski, A.E., Field, L.P., Kemp, S.J., Mounteney, I., Bernal, S.A., Corkhill, C.L., Hyatt, N.C., Provis, J.L., Black, L., 2015. Demonstration of carbonation of the NRVB. Natl. Nucl. Lab. 16 NNL (14) 13296 Issue 4.

Hicks, T.W., Baldwin, T.D., Hooker, P.J., Richardson, P.J., Chapman, N.A., McKinley, I.G., Neall, F.B., 2008. Concepts for the Geological Disposal of Intermediate-level Radioactive Waste. Report no. 0736–1. pp. 1–66.

Hoch, A.R., Baston, G.M.N., Glasser, F.P., Hunter, F.M.I., Smith, V., 2012. Modelling evolution in the near field of a cementitious repository. Mineral. Mag. 76, 3055–3069. http://dx.doi.org/10.1180/minmag.2012.076.8.21.

Holland, T.R., Tearle, W.M., 2003. Serco assurance a review of NRVB mineralogy. Serco Assur SERCO/ERRA-0455 January.

Hooper, A.J., 1998. Repository for radioactive waste-vault backfill. Patent number: 5,740, 546.

Iler, R.K., 1973. The effect of particle size on the solubility of amorphous silica in water. J. Phys. Chem. 43, 399–408. http://dx.doi.org/10.1021/j150557a024.

Jansen, D., Goetz-Neunhoeffer, F., Lothenbach, B., Neubauer, J., 2012. The early hydration of Ordinary Portland Cement (OPC): an approach comparing measured heat flow with calculated heat flow from QXRD. Cem. Concr. Res. 42, 134–138. http://dx.doi.org/10.1016/j.cemconres.2011.09.001.

Kantro, D.L., 1980. Influence of water reducing admixtures on properties of cement paste - a Miniature Slump Test. Cem. Concr. Aggregates 2, 95–102.

Landis, E.N., Keane, D.T., 2010. X-ray microtomography. Mater. Charact. 61, 1305–1316. http://dx.doi.org/10.1016/j.matchar.2010.09.012.

Lothenbach, B., Le Saout, G., Gallucci, E., Scrivener, K., 2008. Influence of limestone on the hydration of Portland cements. Cem. Concr. Res. 38, 848–860. http://dx.doi.org/10.1016/j.cemconres.2008.01.002.

Lothenbach, B., Winnefeld, F., Alder, C., Wieland, E., Lunk, P., 2007. Effect of temperature on the pore solution, microstructure and hydration products of Portland cement pastes. Cem. Concr. Res. 37, 483–491. http://dx.doi.org/10.1016/j.cemconres.2006.11.016.

Menéndez, G., Bonavetti, V., Irassar, E.F., 2003. Strength development of ternary blended cement with limestone filler and blast-furnace slag. Cem. Concr. Compos 25, 61–67. http://dx.doi.org/10.1016/S0958-9465(01)00056-7.

Nuclear Decommissioning Authority, 2015. Geological Disposal the 2013 Derived Inventory. Report no. NDA/RWM/120. .

Nuclear Decommissioning Authority, 2010a. Geological Disposal: an Overview of the Generic Disposal System Safety Case. NDA Report no. NDA/RWMD/010. .

Nuclear Decommissioning Authority, 2010b. Geological Disposal: Near-field Evolution Status Report. Report no. NDA/RWMD/033. Nuclear Decommissioning Authority.

Nuclear Decommissioning Authority, 2010c. Retrievability of Waste Emplaced in a Geological Disposal Facility. Doc No RWMDPP03 December. Nuclear Decommissioning Authority.

Radioactive Waste Management, 2016. RWM HAW Innovation and Delivery: a Review of Cement Powders Security of Supply, Specifications and Disposability Issues. Report no. NDA/RWM/144. Nuclear Decommissioning Authority.

Richardson, I.G., 2008. The calcium silicate hydrates. Cem. Concr. Res. 38, 137–158. http://dx.doi.org/10.1016/j.cemconres.2007.11.005.

Richardson, I.G., Black, L., Skibsted, J., Kirkpatrick, R.J., 2010. Characterisation of cement hydrate phases by TEM, NMR and Raman spectroscopy. Adv. Cem. Res. 22, 233–248. http://dx.doi.org/10.1680/adcr.2010.22.4.233.

Scrivener, K., Snellings, R., Lothenbach, B., 2016. A Practical Guide to Microstructural

Analysis of Cementitious Materials. CRC Press, Taylor & Francis Group.

Scrivener, K.L., Juilland, P., Monteiro, P.J.M., 2015. Cement and concrete research advances in understanding hydration of Portland cement. Cem. Concr. Res. http://dx.doi.org/10.1016/j.cemconres.2015.05.025.

Sun, J., 2011. Carbonation Kinetics of Cementitious Materials Used in the Geological Disposal of Radioactive Waste. PhD thesis. . http://discovery.ucl.ac.uk/1306875/.

Swanton, S.W., Heath, T.G., Clacher, A., 2016. Leaching behaviour of low Ca:Si ratio CaO–SiO2–H2O systems. Cem. Concr. Res. 88, 82–95. http://dx.doi.org/10.1016/j.cemconres.2016.06.001.

Taylor, H.F. (Ed.), 1997. Cement Chemistry, second ed. Thomas Telford Publishing.

United Kingdom Nirex Limited, 2005. Context Note 4.1: Retrievability. United Kingdom Nirex Ltd Number: 484424 December.